Uwe Reisgen • Dietmar Drummer

Enhanced Material and Part Optimization and Process Intensification

Proceedings of the third International Joint Conference on

Enhanced Material and Part Optimization and Process Intensification EMPOrIA 2026

02^{nd} and 03^{rd} of June 2026, Aachen, Germany

Editors

Uwe Reisgen
RWTH Aachen University
Welding and Joining Institute
Germany

Dietmar Drummer
Friedrich-Alexander-Universität Erlangen-Nürnberg
Institute of Polymer Technology
Germany

Uwe Reisgen, Dietmar Drummer (eds.)

EMPOrIA 2026

Proceedings of the third International Joint Conference on Enhanced Material and Part Optimization and Process Intensification

Shaker Verlag
Düren 2026

Bibliographic information published by the Deutsche Nationalbibliothek
The Deutsche Nationalbibliothek lists this publication in the Deutsche Nationalbibliografie; detailed bibliographic data are available in the Internet at http://dnb.d-nb.de.

Shaker Verlag 2026

Print-ISBN 978-3-8191-0730-6
PDF-ISBN 978-3-8191-0670-5
https://doi.org/10.2370/9783819106705

Shaker Verlag GmbH • Am Langen Graben 15a • 52353 Düren
Phone: 0049/2421/99011-0 • Telefax: 0049/2421/99011-9
Internet: www.shaker.de • e-mail: info@shaker.de

Date: 31.03.2026

Adaptive Process Control Strategies For Variable Wall Thickness In Laser Metal Deposition: A Framwork Utilizing Articifical Neural Networks

H. Kruse*, A. Kulkarni, G. Menezes de Souza Melo, M. Sudmanns, J.-H. Schleifenbaum

RWTH Aachen University, Chair for Digital Additive Production, Campus-Boulevard 73, 52074, AACHEN, GERMANY

*Corresponding author: E-mail: henrik.kruse@dap.rwth-aachen.de ORCID: 0000-0001-5674-2634

Abstract

Laser Metal Deposition (LMD) offers significant potential for optimizing local component properties through local reinforcement or coating, enabling enhanced performance and functionality. It is widely applied in repair and remanufacturing, where precise control of material deposition is essential for restoring component geometry. However, achieving high geometric accuracy requires robust process control strategies and a systematic link between target geometry and process parameters.

In this context, this paper presents a data-driven approach to realize variable wall thickness in LMD based on an artificial neural network (ANN). A multilayer feed-forward network is trained on a combined dataset of experimental measurements and FEM-based simulations to capture the relationship between process parameters and meltpool geometry. The model is embedded in an inverse optimization framework to determine process parameters for predefined target geometries. Experimental validation on a demonstrator confirms controlled variation of track width at approximately constant height, demonstrating improved dimensional controllability and process efficiency.

Keywords
Additive Manufacturing (AM), Laser Metal Deposition (LMD), Machine Learning (ML), Remanufacturing

1 Introduction

Laser Metal Deposition (LMD) has become an established additive manufacturing process for the fabrication, repair, and functional enhancement of metallic components, particularly in tooling and turbomachinery applications [1,2]. Its capability to locally add material makes it especially suitable for applications requiring tailored material distribution or geometry adaptation.

However, the reliable manufacturing of geometrically accurate structures remains a major challenge in LMD [3]. Due to the layer-wise deposition of overlapping melt tracks, local deviations in material accumulation frequently occur. Excess material deposition leads to surface irregularities and dimensional inaccuracies, while insufficient deposition in regions with complex geometries can result in pores or incomplete filling of the target geometry. These effects limit the achievable dimensional accuracy and reproducibility of the process.

A key challenge lies in the lack of a direct relationship between desired track geometry and the corresponding process parameters. In conventional approaches, parameter selection is largely based on empirical knowledge or simplified assumptions, requiring extensive experimental effort.

Toolpath planning strategies are commonly used to improve process quality and can be divided into offline and online approaches [4,5]. While online approaches enable real-time adaptation based on sensor feedback and are therefore considered highly promising, their industrial application remains challenging due to sensor limitations, process complexity, and restricted controllability of certain parameters. In particular, the powder mass flow rate cannot be adjusted with sufficient temporal resolution during deposition. As a result, effective process control is primarily achieved through laser power and scanning speed.

Consequently, offline process planning remains widely used in industrial practice. Enhancing these approaches with predictive models enables a systematic adaptation of process parameters along the toolpath without requiring real-time feedback [6].

Machine learning approaches have been investigated to capture complex and nonlinear relationships in LMD processes [7–9]. However, most existing studies focus on monitoring or defect detection, while the direct prediction of process parameters for a predefined geometry, particularly in an inverse formulation, remains insufficiently explored [10,11].

2 Aim of the Investigation

Achieving high geometric accuracy in LMD requires a systematic link between target geometry and process parameters. Building on previous work of the authors, in which a finite element model (FEM) was developed to predict melt pool geometry, this study extends the approach toward geometry-driven process control [12–14].

The objective of this work is to enable the prediction of process parameters for a predefined single-track geometry using a data-driven surrogate model. For this purpose, an artificial neural network is trained on a combined dataset of simulation and experimental data, capturing both physically consistent trends and real-process variability.

The trained model is coupled with an inverse optimization strategy to determine suitable process parameters for a given target geometry, establishing a continuous pipeline from geometry definition to parameter selection.

The capability of the proposed approach is demonstrated by the realization of a variable wall thickness with predicted process parameters in single-track deposition. The results highlight the potential of machine-learning-assisted process parameter prediction to improve geometric accuracy and process stability and underline its relevance as a building block for future geometry-aware toolpath planning strategies in LMD.

3 Materials and Experimental Details

3.1 Data Generation via FEM and Experiments

To establish a data-driven relationship between process parameters and resulting track geometry, a sufficiently large and consistent dataset is required. In this work, this requirement is addressed by combining experimental measurements with simulation-based data generation.

The simulation data are obtained from a finite element model of the LMD process which was developed and continuously refined in previous work of the authors [12–19]. The model describes track formation as a coupled thermo-physical problem, accounting for heat conduction, mass addition, and free surface evolution based on the Young–Laplace equation with mass conservation. Powder particles are treated as a volumetric heat source or sink depending on their thermal state and interaction with the melt pool. A detailed mathematical description can be found in previous publications [12]. Due to the high computational cost of fully transient simulations, a quasi-stationary approach is applied, enabling efficient evaluation of large parameter spaces while maintaining sufficient accuracy.

Figure 1 shows a comparison between the simulated temperature distribution of a representative single track and the corresponding experimental cross section in the YZ plane. Deviations between simulated and experimentally measured melt pool width, depth, and height remain below 10 %, confirming the validity of the model for data generation [13].

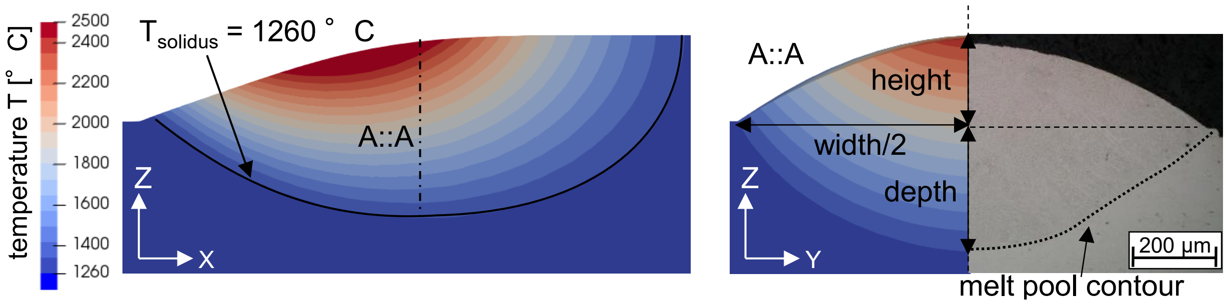

Figure 1: left: side view of the temperature distribution of an exemplary single track simulation, right: YZ cross section perpendicular to the scan velocity along A::A and overlay with optical microscopy [12,13]

An important model extension is the incorporation of powder shielding effects. The attenuation of the laser beam by the powder jet is considered by adapting the local energy input based on empirical particle distributions [20,21].

To enable high-throughput data generation, a fully automated simulation workflow is implemented. The workflow includes parameter generation based on a design of experiments (DoE), simulation execution, and automated extraction of melt pool geometries. Although the FEM solver itself operates sequentially, multiple simulations are executed in parallel at the process level. Using this approach, a total of 2,160 steady-state simulation cases are evaluated within a structured parameter sweep. In this study, Inconel (IN625) was used as the deposited material and stainless steel as the substrate, with temperature-dependent thermophysical properties obtained from manufacturer datasheets (Special Metals), ASM Handbooks, and the NIST database [22].

The investigated DoE spans laser power in the range of 1000 W and 3000 W, scanning speed between 6.7 mm/s and 36.7 mm/s, and powder feed rates between 15 g/min and 30 g/min, covering the relevant process window for stable single-track deposition reported in literature for laser-based deposition of IN625 [23–25].

In addition to simulation data, experimental measurements from single-track depositions are incorporated. The experiments are carried out on an Okuma MU-6300V LASER EX machine equipped with a Trumpf Yb:YAG disk laser operating at a wavelength of 1030 nm and a maximum laser power of 4000 W. A Gaussian beam profile with a laser spot diameter of 3 mm is used. The deposition is performed using a ring-gap nozzle with argon as shielding gas, processing IN625 powder on steel. The experimental parameter space covers scanning speeds between 6.7 mm/s and 33.3 mm/s, laser power between 800 W and 2200 W, and powder mass flow rates between 12 g/min and 18 g/min. In total, 151 cross-sectional samples are generated and prepared metallographically. The resulting melt pool geometries are evaluated using optical microscopy to determine track width, depth, and height.

3.2 Data Processing

Data cleaning is performed to ensure physical consistency and robustness of the dataset. Non-physical simulation results, such as unstable melt pool formations or numerical artifacts, are removed. Additionally, statistical outliers are filtered using an interquartile range (IQR) method to eliminate extreme values that are not representative of stable process conditions. Only samples with complete geometric information are retained. After data cleaning, the final dataset consists of 1,869 valid samples, including 1,805 simulation-based data points and 64 experimental samples.

3.3 ANN Surrogate Model and Optimization Framework

To approximate the nonlinear relationship between process parameters and melt pool geometry, data-driven regression models are investigated. Different model configurations and preprocessing strategies are evaluated to identify a suitable representation of the process behavior. A systematic comparison of several regression algorithms further confirmed that the multilayer perceptron combined with standard z-score scaling provides the most reliable representation of the process behaviour, whereas linear models were unable to capture the strong nonlinear coupling between parameters and meltpool geometry, in agreement with thermo-physical analyses of DED track formation reported by Perani et al [8].

Based on this analysis, a multilayer perceptron (MLP) is selected as the most reliable surrogate model. The network consists of four hidden layers with a 256–128–64–32 neuron topology. Rectified linear unit (ReLU) activation functions are used in the hidden layers, while the output layer remains linear to enable regression of continuous geometric variables. The model is trained using supervised learning on the combined dataset. To improve generalization, L2 regularization is applied, and the dataset is split into training and validation subsets using an 80/20 ratio with a fixed random seed. Different data scaling approaches are evaluated, and standardized normalization is selected to ensure stable training behavior.

The input vector of the forward ANN model consists of the relevant process parameters, including laser power, scanning speed, absorptivity, spot diameter, powder feed rate, and powder efficiency. The output vector represents the resulting melt pool geometry in terms of width, depth, and height. All input and output variables are normalized using a z-score transformation to ensure balanced learning across different feature scales. To represent systematic differences between simulation derived and experimental data, a binary indicator $IS_{exp} \in \{0,1\}$ is included, where $IS_{exp} = 0$ denotes simulation data and $IS_{exp} = 1$ experimental data, enabling the model to account for domain-specific deviations.

Model performance is evaluated using the coefficient of determination (R^2) and the mean absolute error (MAE). Once trained, the ANN serves as a computationally efficient surrogate model. This significantly reduces the need for computationally expensive FEM simulations during process design.

To enable geometry-driven process parameter selection, the trained forward ANN is embedded into an inverse optimization framework, where the surrogate model is iteratively queried to identify parameter sets that reproduce a desired target geometry, as illustrated in Figure 2.

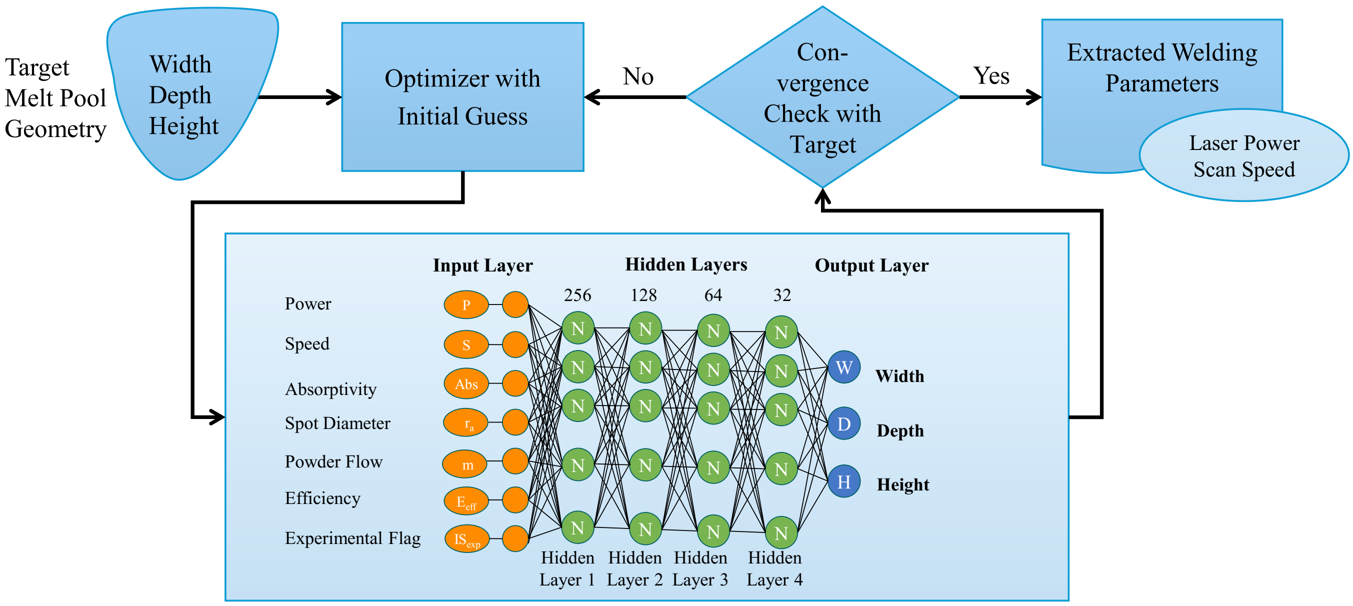

Figure 2: Schematic representation of the optimization framework developed for geometry-driven process parameter selection

The optimization starts from an initial guess within a predefined process window, where parameter bounds are set based on physically feasible ranges from the calibration study. An initial population of candidate parameter sets is generated via stochastic sampling and iteratively evolved by the optimizer. The resulting melt pool geometry is evaluated using the ANN surrogate model and compared to the target geometry, with the population updated until the deviation is minimized. The final solution represents a physically consistent set of process parameters to achieve the desired melt pool geometry.

4 Results and Discussion

The following sections present the main results of this study with respect to the proposed framework for geometry-driven process parameter selection. The evaluation focuses on four key aspects: the acceleration of FEM-based data generation, the predictive accuracy of the surrogate model, the capability of the inverse optimization for geometry-based parameter prediction, and the experimental validation of the predicted parameters, including the realization of variable wall thickness.

4.1 Acceleration of FEM-Based Data Generation

A central contribution of this work is the significant improvement in computational efficiency of the FEM model of the melt pool formation through workflow automation and process-level parallelization. Through parallel execution of multiple simulation instances and optimization of the numerical workflow, the total runtime for approximately 50 parameter sets was reduced to approximately 8–10 h from around 150h.

This corresponds to an overall speedup factor of approximately 20–25, while maintaining the physical fidelity of the model. The improved efficiency enabled the systematic evaluation of more than 2,000 parameter combinations within a feasible time frame, which would not have been practical using the initial simulation setup. In addition, the integration of extended physical effects, such as powder shielding, further improved the consistency of the simulation results without increasing computational costs significantly.

4.2 Surrogate Model Accuracy for Melt Pool Geometry Prediction

Based on the dataset generated, a surrogate modeling framework was established to approximate the relationship between process parameters and melt pool geometry. The predictive performance of the trained ANN is evaluated on an unseen test dataset.

Figure 3a shows the training history of the selected model, where the loss decreases rapidly during the initial epochs and converges towards a stable plateau after approximately 200 epochs without divergence, indicating stable training behavior and effective regularization.

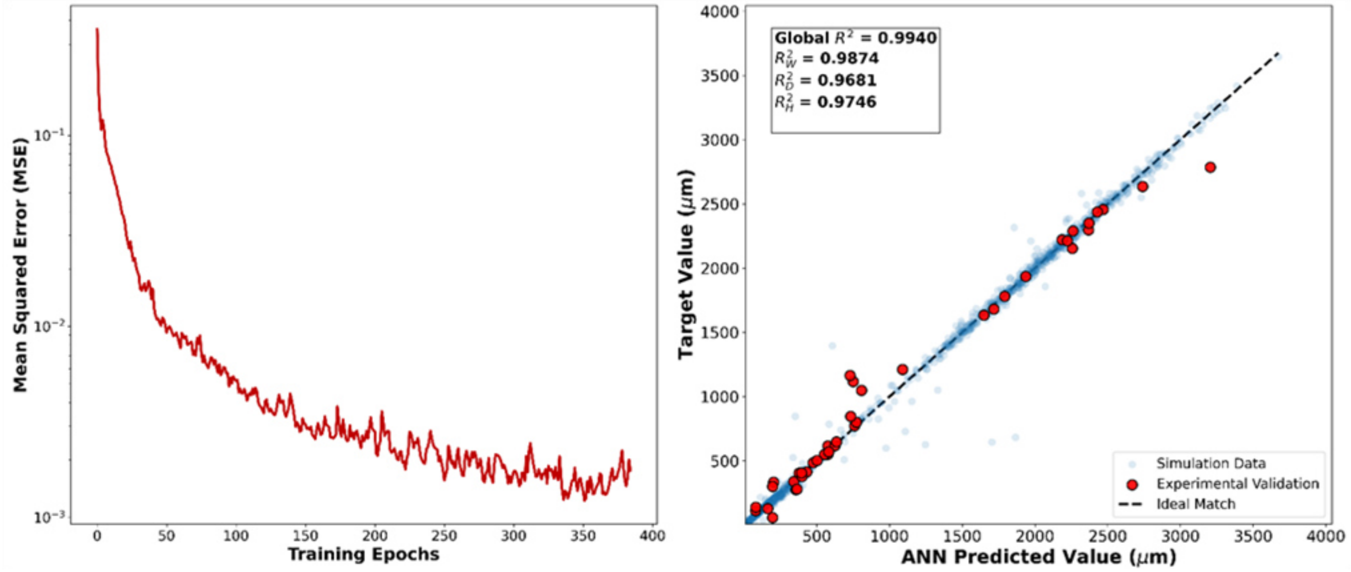

Figure 3: (a) Loss curve during training of the retained MLP (b) Combined parity plot showing predicted vs reference values

The predictive performance is illustrated in the combined parity plot in Figure 3b, showing the agreement between predicted and reference values for the summarized collection of melt pool geometries (width, depth, and height). The model achieves an overall coefficient of determination of $R^2 = 0.994$, demonstrating that the surrogate captures the dominant process relationships across the investigated parameter range. This behavior suggests that the applied normalization and regularization strategy effectively limits overfitting, which has been identified as a frequent challenge in deep-learning-based DED models [10].

A more detailed evaluation of the single melt pool predictions is summarized in Table 1. The model achieves R^2 values of 0.9681 for depth, 0.9874 for width, and 0.9746 for height, with corresponding mean absolute errors of 10.4 µm, 27.9 µm, and 48.7 µm. Over 93 % of all predictions lie within the ±100 µm tolerance band defined by the experimental measurement uncertainty. These values are comparable to, and slightly higher than, the maximum $R^2 = 0.975$ reported by Sarparast for a combined FEM–ANN morphology prediction framework et al. (2025) [27].

Table 1: The prediction metrics for each melt pool dimension.

Target	R^2	MAE(µm)	% ±100	Max |Resid| (µm)
Depth	0.9681	10.4	**98.9 %**	195
Width	0.9874	27.9	**96.5 %**	756
Height	0.9746	48.7	**93.3 %**	1 202

In summary the highest prediction accuracy is observed for melt pool depth. Melt pool width is also predicted reliably, while larger deviations are observed for melt pool height. This difference arises from the underlying formation mechanisms. Depth and width are mainly governed by thermal input and therefore show a more stable dependency on the process parameters. In contrast, track height is strongly influenced by the effective mass input into the melt pool, which introduces additional variability and makes accurate prediction more challenging. This includes not only the nominal powder mass flow rate but also the interaction between powder particles, melt pool dynamics, and gas flow conditions. These effects introduce additional variability, which is only partially captured in the available training of FEM data. As a result, the relationship between process parameters and track height exhibits increased complexity and variability, leading to reduced prediction accuracy compared to depth and width.

Residual analysis confirms that the prediction errors are centred around zero with no systematic bias, indicating good generalization across the investigated geometry range. Overall, the achieved accuracy demonstrates that the surrogate model provides a reliable forward approximation of the process and is sufficiently accurate for use in inverse parameter optimization.

4.3 Inverse Optimization Results

The capability of the proposed framework to determine process parameters for predefined target geometries is evaluated using the inverse optimization approach.

Representative results for low, medium, and high-power conditions are summarized in Table 2. For each predefined target geometry, the inverse optimization determines a corresponding set of process parameters using the inverse ANN surrogate model. The resulting parameter sets are subsequently used to predict the melt pool geometry, and these predictions are compared with FEM simulations and experimental measurements.

Across all investigated cases, the predicted melt pool width shows small deviations, typically within +1–2 % compared to experimental results. This accuracy is comparable to the AIDED framework proposed by Shang et al. (2025) [26], who reported relative errors of 1.75 % for track width and 12.04 % for height during parameter recovery. The melt pool depth exhibits moderate deviations, particularly in the low-power regime, where small variations in energy input have a strong influence on penetration behavior. The largest deviations are observed for melt pool height, with errors up to approximately 30–40 %, reflecting the known sensitivity of reinforcement to powder-related effects.

Despite these deviations, the predicted geometries follow the expected trends across the parameter range investigated. Furthermore, all optimized parameter sets remain within the physically consistent operating window defined by the calibration study, indicating that the inverse optimization produces feasible and stable solutions.

Table 2: Inverse Optimization Results

Parameter	Case 1 (Low power)	Case 2 (Mid power)	Case 3 (High power)
Target (W/D/H)	1800/150/600	2000/300/800	2500/450/800
Power (W)	1000	1587.6	2074
Speed (mm/s)	23.83	33.33	26.67
Absorptivity (%)	50	50	50
Powder efficiency (%)	60	60	70
Predicted (W/D/H)	1698/126/818.2	2075/289.6/980	2444.8/490/819.2

Experimental Power (W)	1000	1600	2000
Experimental Speed (mm/s)	23.23	33.33	26.67
Experimental (W/D/H)	1673/150/733	2051/252/537	2393/498/636
Error Width (%)	+1.5	+1.2	+2.2
Error Depth (%)	-16.0	+14.9	-1.6
Error Height (%)	+11.6	+42.5	+28.8

4.4 Experimental Validation and Demonstration of Variable Wall Thickness

To validate the practical applicability of the proposed framework, the predicted process parameters are transferred to single-track deposition experiments. Figure 4 shows a representative single-track experiment, where the track width is continuously varied over a length of 36 mm while maintaining an approximately constant track height of about 200 µm. The profilometry data demonstrates a deviation of approximately 26 µm, corresponding to a relative error below 13%, while the track width is adjusted over a wide range. Within this configuration, a controllable width range from 0.9 mm to 1.95 mm is achieved, corresponding to an adjustment factor of 2.2. This confirms that width and height can be decoupled to a significant extent by appropriate parameter selection.

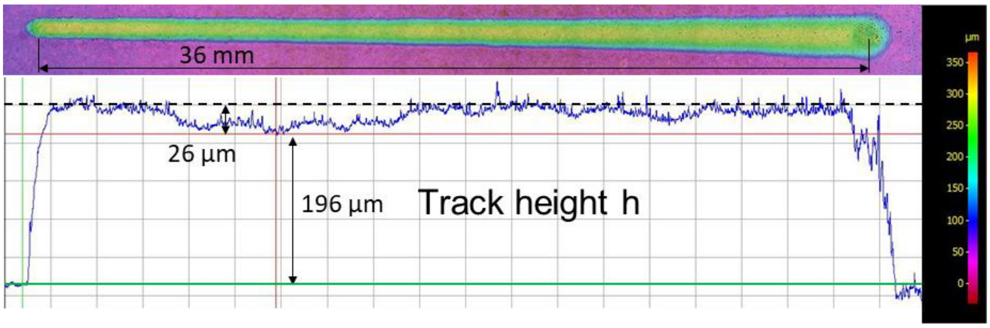

Figure 4: Profilometry of a melt track with variable width (between 1mm to 3mm) and constant track height (error <13%)

Beyond this representative example, additional validation experiments were conducted at different height levels and process conditions. For a second parameter set, a width range from 1914 µm to 2500 µm is obtained at approximately 500 µm track height, corresponding to a factor of 1.31. At a higher track height of approximately 900 µm, the adjustable width range increases to 1696 µm to 2772 µm, corresponding to a factor of 1.63.

These results demonstrate that, in contrast to conventional parameter selection, where the resulting geometry is largely determined by a fixed process equilibrium, the proposed framework enables a targeted and reproducible adjustment of track width at approximately constant track height. Across all investigated configurations, the achievable degree of geometric controllability is significantly increased, with an improvement factor of up to 2.2 in terms of targeted dimensional adjustment.

Although deviations remain, particularly for melt pool height due to variations in powder delivery and local process conditions, the overall geometric trends are reproduced reliably. These findings confirm that the proposed framework provides a viable basis for geometry-driven process control and represents a key step towards adaptive toolpath strategies for variable wall thickness manufacturing in LMD.

5 Summary

This work presents a data-driven framework for geometry-based process parameter selection in Laser Metal Deposition (LMD), enabling the controlled variation of track geometry and the realization of variable wall thickness. By combining an improved FEM-based simulation workflow with process-level parallelization, a large and consistent dataset was generated with a computational speedup of approximately 20–25. Based on this dataset, an artificial neural network was trained to predict melt pool geometry from process parameters with high accuracy, achieving R^2 values up to 0.99 and predictions largely within the experimental tolerance of ±100 µm.

The trained model was further integrated into an inverse optimization framework, allowing the determination of process parameters for predefined target geometries. The results show good agreement between predicted, simulated, and experimental geometries, particularly for melt pool width. Experimental validation confirms that the predicted parameters can be transferred to real process conditions, enabling controlled variation of track width at approximately constant track height. This results in a significant improvement in dimensional controllability, with an adjustable width range corresponding to a factor of up to 2.2.

Despite these results, limitations remain, particularly regarding the reduced prediction accuracy for melt pool height due to the influence of powder-related effects and local process variations, as well as the restriction to single-track validation. Future work will focus on extending the experimental dataset, improving the representation of material deposition effects, and transferring the approach to multi-layer and geometry-dependent process control. For application to more complex geometries, layer-to-layer interactions, heat accumulation, and geometry-dependent process variations must be considered, along with integration into toolpath planning strategies. In addition, automated acquisition of track geometry is required to further reduce the effort for data generation and increase model versatility.

Acknowledgements

All presented investigations were conducted in the context of the Collaborative Research Centre SFB1120 "Precision Melt Engineering" at RWTH Aachen University and funded by the German Research Foundation (DFG). For the sponsorship and the support, we wish to express our sincere gratitude.

Conflict of Interest

The author declares no conflict of interest.

Data Availability Statement

The data that support the findings of this study are available at http://hdl.handle.net/21.11102/56ea1ed7-9bca-4912-930c-fcd08b86c671 upon request.

References

[1] A. Gasser, G. Backes, I. Kelbassa, A. Weisheit, K. Wissenbach, Laser Metal Deposition (LMD) and Selective Laser Melting (SLM) in Turbo-Engine Applications, LTJ 7 (2010) 58–63. doi:10.1002/latj.201090029.

[2] D.-G. Ahn, Directed Energy Deposition (DED) Process: State of the Art, Int. J. of Precis. Eng. and Manuf.-Green Tech. 8 (2021) 703–742. doi:10.1007/s40684-020-00302-7.

[3] A. Dass, A. Moridi, State of the Art in Directed Energy Deposition: From Additive Manufacturing to Materials Design, Coatings 9 (2019) 418. doi:10.3390/coatings9070418.

[4] Y.-Y. Chang, J.-R. Qiu, Y.-X. Chen, S.-J. Hwang, Research on deposition toolpath planning and laser head Z-axis rising height setting for directed energy deposition, Optics & Laser Technology 161 (2023) 109198. doi:10.1016/j.optlastec.2023.109198.

[5] J. Jiang, Y. Ma, Path Planning Strategies to Optimize Accuracy, Quality, Build Time and Material Use in AM: A Review, Micromachines (Basel) 11 (2020). doi:10.3390/mi11070633.

[6] M.-N. Bold, N. Pirch, S. Ziegler, J.H. Schleifenbaum, Evaluation of Offline Path Planning for Laser Metal Deposition on Freeform Surfaces, in: Lasers in Manufacturing, München, 2019.

[7] M. Gihr, A. Rashid, S.N. Melkote, Bead geometry prediction and optimization for corner structures in directed energy deposition using machine learning, Additive Manufacturing 84 (2024) 104080. doi:10.1016/j.addma.2024.104080.

[8] M. Perani, S. Baraldo, M. Decker, A. Vandone, A. Valente, B. Paoli, Track geometry prediction for Laser Metal Deposition based on on-line artificial vision and deep neural networks, Robotics and Computer-Integrated Manufacturing 79 (2023) 102445. doi:10.1016/j.rcim.2022.102445.

[9] D. Knüttel, S. Baraldo, A. Valente, F. Bleicher, K. Wegener, E. Carpanzano, Machine learning based track height prediction for complex tool paths in direct metal deposition, CIRP Annals 71 (2022) 193–196. doi:10.1016/j.cirp.2022.03.032.

[10] D.W. Rosen, X. Liu, Selected applications of artificial intelligence and machine learning in metal additive manufacturing, Weld World (2026). doi:10.1007/s40194-026-02335-z.

[11] F. Hermann, B. Chen, G. Ghasemi, V. Stegmaier, T. Ackermann, P. Reimann, S. Vogt, T. Graf, M. Weyrich, A Digital Twin Approach for the Prediction of the Geometry of Single Tracks Produced by Laser Metal Deposition, Procedia CIRP 107 (2022) 83–88. doi:10.1016/j.procir.2022.04.014.

[12] J. Zielinski, A holistic approach to understand laser additive manufacturing from melt pool to microstructure. Dissertation, 2022.

[13] J. Zielinski, H. Kruse, M.-N. Bold, G. Boussinot, M. Apel, J.H. Schleifenbaum, Melt Pool Formation and Out-of-Equilibrium Solidification During the Laser Metal Deposition Process (2021) 113–122. doi:10.1007/978-3-030-70332-5_11.

[14] N. Pirch, S. Linnenbrink, A. Gasser, K. Wissenbach, R. Poprawe, 2017. Analysis of track formation during laser metal deposition. Journal of Laser Applications 29, 022506. doi:10.2351/1.4983231.

[15] N. Pirch, M. Niessen, S. Linnenbrink, T. Schopphoven, A. Gasser, R. Poprawe, C. Schöler, D. Arntz, W. Schulz, 2018. Temperature field and residual stress distribution for laser metal deposition. Journal of Laser Applications 30, 032503. doi:10.2351/1.5040634.

[16] N. Pirch, H. Schleifenbaum, S. Linnenbrink, A. Gasser, R. Poprawe, M. Niessen, Influence of process strategy on distortion and residual stresses for the powder based laser metal deposition process, Materialwissenschaft Werkst 48 (2017) 1304–1313. doi:10.1002/mawe.201700169.

[17] M.-N. Bold, S. Linnenbrink, N. Pirch, A. Gasser, J. Mund, J.H. Schleifenbaum, Powder based laser material deposition on edges, Journal of Laser Applications 32 (2020) 32001. doi:10.2351/7.0000095.

[18] N. Pirch, S. Linnenbrink, A. Gasser, H. Schleifenbaum, Laser-aided directed energy deposition of metal powder along edges, International Journal of Heat and Mass Transfer 143 (2019) 118464. doi:10.1016/j.ijheatmasstransfer.2019.118464.

[19] M.-N. Bold, S. Ziegler, J. Zielinski, J.H. Schleifenbaum, Study Of Laser Metal Deposition Of In718 On Inclined Planes: Influence Of Inclination On Height And Width Of Deposited Material, in: Metal Additive Manufacturing Conference 2019, Wien, Austria, 2019.

[20] S. Ye, S. Benito, A. Berger, S. Weber, Development of a 3D multi-scale PBF-LB/M temperature history FEM simulation model, Int J Adv Manuf Technol (2025). doi:10.1007/s00170-025-16895-9.

[21] H. Qi, J. Mazumder, H. Ki, 2006. Numerical simulation of heat transfer and fluid flow in coaxial laser cladding process for direct metal deposition. Journal of Applied Physics 100, 024903. doi:10.1063/1.2209807.

[22] S. Saha, O.L. Kafka, Y. Lu, C. Yu, W.K. Liu, Microscale Structure to Property Prediction for Additively Manufactured IN625 through Advanced Material Model Parameter Identification, Integr. Mater. Manuf. Innov. 10 (2021). doi:10.1007/s40192-021-00208-5.
[23] D.R. Feenstra, A. Molotnikov, N. Birbilis, Utilisation of artificial neural networks to rationalise processing windows in directed energy deposition applications, Materials & Design 198 (2021) 109342. doi:10.1016/j.matdes.2020.109342.
[24] F. Zafar, O. Emadinia, J. Conceição, M. Vieira, A. Reis, A Review on Direct Laser Deposition of Inconel 625 and Inconel 625-Based Composites—Challenges and Prospects, Metals 13 (2023) 787. doi:10.3390/met13040787.
[25] J.P. Rodrigues, R.S. Thanumoorthy, S.K. Manjhi, P. Sekar, D.A. Perumal, S. Bontha, A. Balan, Hybrid additive manufacturing of ER70S6 steel and Inconel 625, Materials Today Communications 37 (2023) 106977. doi:10.1016/j.mtcomm.2023.106977.
[26] X. Shang, A. Talbot, E. Li, H. Wen, T. Lyu, J. Zhang, Y. Zou, Accurate inverse process optimization framework in laser directed energy deposition, Additive Manufacturing 102 (2025) 104736. doi:10.1016/j.addma.2025.104736.